International Journal on Communications Antenna and Propagation (I.Re.C.A.P.), Vol. 10, N. 5
ISSN 2039 – 5086
October 2020

Graphene-Controlled Reconfigurable Patch Antenna Using Shorting Elements

A. Lovascio[1], V. Centonze[2], A. D'Orazio[1], M. Grande[1]

Abstract – *This paper reports the design of a patch antenna that uses of graphene-based shorting elements to implement advanced functionalities, such as multi-band and beam-steering, which make it extremely attractive for the future Fifth-Generation (5G) wireless networks. The proposed structure has 36.75×29.25 mm^2 size and it has been designed on a Rogers RT/duroid 5880 substrate, 1.58 mm thick. It is composed by an external slotted rectangular patch that contains an internal circular shape. The internal shape is separated from the external one by a circular slot but it is linked to it by four copper bridges short-circuited to the underlying ground plane through a thin metal pin, one for each bridge. It has been shown that the multi-band and the beam-steering functionalities are strongly affected by the geometric location of the shorting pins. By controlling the connection of the bridges perpendicular to the antenna length, the direction of the antenna main lobe can be changed. By using the Finite Element Method (FEM), the geometric location of the shorting pins has been optimized so that the antenna resonates at 3.5 GHz frequency, exhibiting a 6.6 dBi maximum gain and a -17.55 dB S_{11} parameter. Moreover, by controlling electronically the connection of the shorting elements using graphene foils, three distinct beams, steering between -22 to +22 degrees, have been obtained. The beams show about 1.4 dBi theoretical antenna gain using graphene foils with 20 Ω/sq sheet resistance.*

Keywords: *Beam Steering, Multi-Band Patch Antenna, Graphene, Shorting Pins, Fifth-Generation (5G)*

Nomenclature

4G	Fourth-Generation
5G	Fifth-Generation
D	Antenna bridge width [mm]
f	Resonance frequency [GHz]
$\mathbf{E}$	Electric field vector [V/m]
FEM	Finite Element Method
$\mathbf{J}$	Current density vector [A/m]
L	Antenna length [mm]
PEC	Perfect Electric Conductor
R_{in}	Radius of the antenna inner shape [mm]
R_{out}	Outer radius of the antenna circular slot [mm]
R_S	Graphene sheet resistance [Ω/sq]
$SOCl_2$	Thionyl chloride
S_{XX}	Scattering parameter [dB]
σ	Graphene conductivity [Ω^{-1}]
W	Antenna width [mm]
X_{obj}	Position of an object on the antenna along the X-axis [mm]
Y_{obj}	Position of an object on the antenna along the Y-axis [mm]

I. Introduction

The 5G wireless networks represent the future of the telecommunication. In the last years, many mobile multimedia services that have led to an exponential increase in throughput and bandwidth demand have been developed [1]. Since the current 4G technology cannot sustain such a demand, research efforts have been focused on the improvement of the network infrastructure in order to allow the 5G applications to have a real impact on the society. In this scenario, the propagation losses, the scattering and the interferences in wireless networks define the main bottlenecks since 5G applications are pushing towards higher operating frequencies (where higher bandwidth will be available) in order to satisfy the throughput demand. High bandwidths are a mandatory step in to target the connectivity goals that aim to achieve tens of Gigabits per second [2]. In order to solve the issues regarding higher propagation losses, one of the hottest research fields regards the so-called smart antennas. The antennas are designed to have new and attractive features, such as multi-band, wideband, and beam-steering capability. The general idea is to optimize the connectivity between the radio base station and the end-user (e.g. smartphone) by pointing the maximum antenna gain along the line-of-sight of two communicating systems. In this way, the power transmission will be maximized in such a

Available online by October 31st, 2020
https://doi.org/10.15866/irecap.v10i5.18080

direction, and the interference with other neighboring wireless systems will be reduced [3]. Recently, different configurations that implement such features have been proposed. Ultra wideband [4]-[8] and multi-band [9]-[11] antennas have been reported in literature for different applications, which are also suitable for 5G networks.

Moreover, antennas with beam-steering property have been proposed based on antenna arrays combined with reconfigurable systems, such as mechanical rotations [3], lens [12] and phase shifters as the Blass matrices [13], [14]. In this paper, an innovative configuration of a patch antenna assisted by graphene-based shorting elements, which realize the beam steering exploiting the tuning properties of graphene, is proposed. Metallic shorting elements, as the shorting pins, in microstrip antennas have been widely studied: they have been exploited for instance to enhance the gain and directivity [15], to decrease the size at lower frequencies [16], [17], to realize dual-band antenna [18], [19] or multi-band [20].

However, no solutions have been proposed to control the radiation direction in the microwave regime using graphene foils. The ability to integrate graphene, a two-dimensional allotrope of carbon [21], into devices has attracted great attention in recent years due to its enormous potential as a mean of achieving the dynamic control of the electromagnetic response [28]. Graphene has been widely exploited for the realization of amplitude or phase modulation in the microwave, THz and near-infrared ranges [22]-[27]. In the microwave regime, graphene has been successfully exploited to realize several proof-of-principle devices spanning from optically transparent polarizers [28], microwave absorbers [29]-[33] to antennas [34]-[36]. The antenna proposed in this paper has been optimized to resonate at 3.5 GHz (frequency exploited in 5G networks). It exhibits multi-band behavior when three or four shorting pins are used. Moreover, the presence of graphene-based elements in the antenna configuration allows controlling electrically the beam direction.

The paper is organized as follows. In Section II, the design of the patch antenna has been described by comparing the performance of three-pin and four-pin configurations. In Section III, the beam-steering capability of the antenna and the graphene-based solution is discussed.

II. Shorting Elements-Based Antenna Design

The proposed patch antenna is composed of two different geometrical elements: an external slotted rectangular patch that contains inner circular slots. The two patches are connected along X-axis direction by a conductive bridge (width equal to D) short-circuited to the ground plane through a thin metallic pin. In authors' previous paper [37], two different configurations have been analyzed: the former with only one pin in the antenna geometry; the latter having two pins. It has been showed that the antenna performance, especially in terms of impedance matching and irradiating frequency, has been sensitive to the location and the geometry of the pins while the feeding probe had a weak influence on the impedance matching. The one-pin antenna has showed dual-band capability at 2.24 GHz (lower resonance frequency) and 8.11 GHz (higher resonance frequency), and it has exhibited the following figures of merit:

- Reflection coefficient at lower resonance: -19.05 dB;
- Reflection coefficient at higher resonance: -29 dB;
- Maximum antenna gain at lower resonance: 7.02 dBi;
- Maximum antenna gain at higher resonance: 6.55 dBi.

However, the capability of the antenna to become single-band when a second pin was introduced in the geometry has been observed. Therefore, the presence/absence of the further conducting pins can change the number of resonances introducing several features to the already excellent performance of the antenna. In this paper, a patch antenna exploiting three and four shorting pins integrated with copper elements is considered. The antennas have been designed considering a Rogers RT/duroid 5880 substrate, 1.58 mm thick. The substrate has 64×57 mm^2 size for the antenna with three shorting pins while a footprint of 67×60 mm^2 for the one with four shorting pins. The antennas have been numerically simulated in COMSOL Multiphysics using the Finite Element Method (FEM) on a wideband frequency region (1-10 GHz). The metallic parts of the antenna have been modelled as Perfect Electric Conductors (PECs). In order to optimize the numerical simulations, two different calculation domains have been implemented. In 1-4.8 GHz frequency range, the simulations have been performed in a spherical calculation domain with a 100 mm radius, implementing a 20 mm thickness Perfect Matched Layer on the borders. In 4.9-10 GHz frequency range, a cylindrical-shape calculation domain of 60 mm height and of 65 mm diameter has been adopted, and a 10 mm thickness Perfect Matched Layer has been used. For both domains, an extremely fine mesh has been adopted for the entire electromagnetic model, setting to 0.7 mm the maximum element size of the mesh only for the antenna top footprint. In this way, the accuracy of the result has been maintained reducing at the same time the computation time. Regarding the frequency discretization, the whole range from 1 to 10 GHz has been simulated with 100 MHz step, refining the simulation with 40 frequency points on a 200 MHz range around on two lower frequency resonances, and with a 10 times smaller frequency step (10-20 MHz) for the higher frequency resonance.

II.1. Three-Pin Antenna Design

Fig. 1(a) depicts the first configuration based on the patch antenna with three shorting pins and three slots.

This antenna has been designed by setting L=36.75 mm, W=29.25 mm, R_{in}=7.4 mm, R_{out}=11.3 mm, D=2.75 mm, X_{pin1}=-9.5 mm (first pin position along X-axis),

X_{pin2}=12 mm (second pin position along X-axis), Y_{pin}=12 mm (third pin position along Y-axis), R_{pin}=1 mm (pin radius, equal for all three pins), X_{feed}=-1.5 mm (feeding probe position along X-axis). The footprint is about 9% smaller than the one reported in [37], i.e. 36.75×29.25 mm^2. The antenna exhibits a three-band behavior, irradiating at 2.187 GHz (S_{11}=-12.75 dB), 3.492 GHz (S_{11}=-17.55 dB) and 9.4 GHz (S_{11}=-35.72 dB) resonance frequencies, as shown in Fig. 1(b). In Figs. 2 and Fig. 3, the radiation pattern for all the resonance frequencies is shown expressed in terms of E-plane (XZ-plane) and H-plane (YZ-plane). In Figs. 4, the maximum antenna gain as function of the frequency is depicted. Figs. 2 show that the radiation pattern at the 3.492 GHz frequency is strongly affected by the location of the third pin since the main lobe direction of the E-plane radiation pattern changes according to the position of the third pin and bridge. In particular, an inclination of about +/-22 degrees in the E-plane radiation pattern has been observed when the third pin is placed at Y=+12 mm and Y=-12 mm, respectively. The total maximum antenna gain is 6.6 dBi for both configurations. The antenna also exhibits a higher resonance frequency at 9.4 GHz with a 2D radiation pattern shown in Fig. 3. The maximum antenna gain at this frequency is equal to 9.83 dBi regardless of the position of the third pin since the current distribution is mainly concentrated in the inner circle.

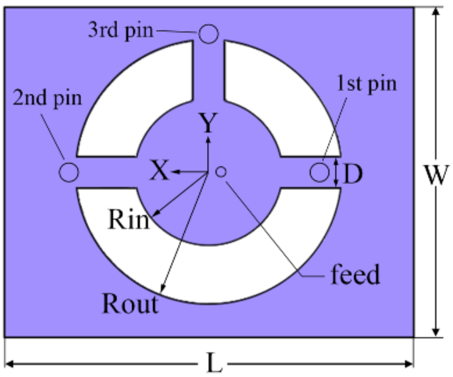

(a)

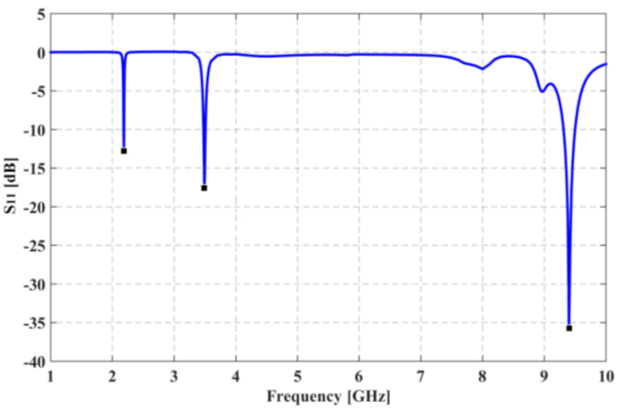

(b)

Figs. 1. Patch antenna with three shorting pins: (a) geometry. (b) Computed scattering parameter S_{11}

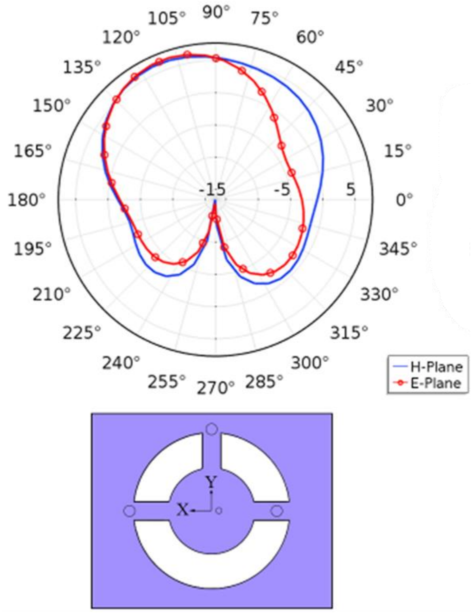

(a)

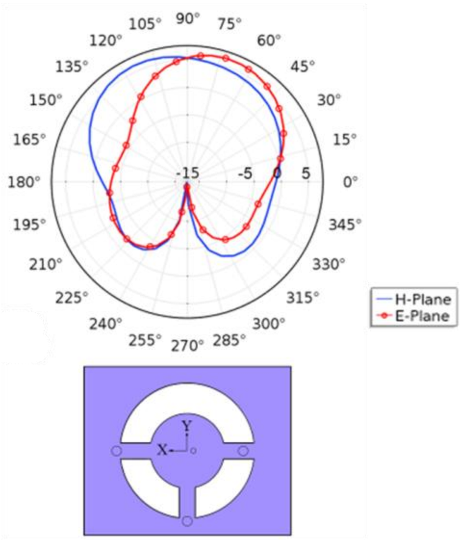

(b)

Figs. 2. Three-pin antenna radiation pattern computed at 3.5 GHz resonance frequency when the third pin position is at (a) Y>0 and at (b) Y<0

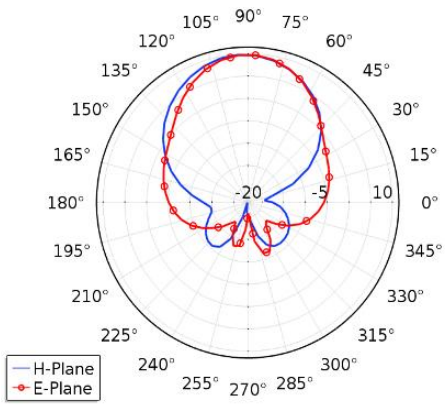

Fig. 3. 3D radiation pattern at 9.4 GHz computed for the three-pin patch antenna

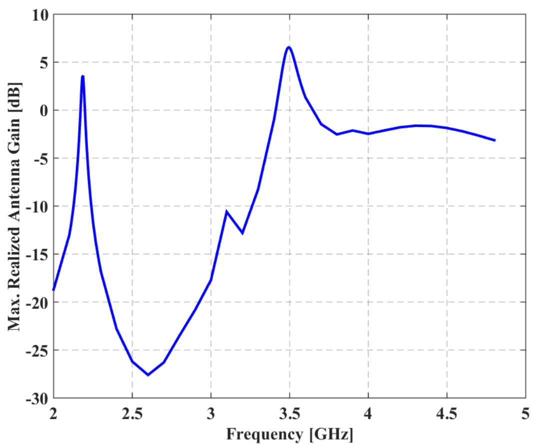

(a)

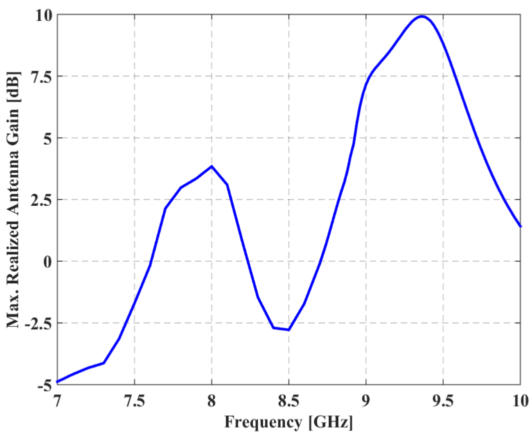

(b)

Figs. 4. Maximum realized antenna gain as function of lower frequencies (a) and higher frequencies (b) computed for the three-pin patch antenna

II.2. Four-Pin Antenna Design

Fig. 5(a) depicts the patch antenna with four metallic shorting pins. It has been designed by setting L=40.75 mm, W=33.25 mm, R_{in}=7.4 mm, R_{out}=13.3 mm, D=2.75 mm, X_{pin1}=-11 mm (first pin position along X-axis), X_{pin2}=14 mm (second pin position), Y_{pin3}=14 mm (third pin position), Y_{pin4}=-14 mm (fourth pin position) R_{pin}=0.9 mm, X_{feed}=-1.5 mm.

The four-pin configuration allows the antenna to have a three-band behavior, irradiating at 2.43 GHz (S_{11}=-22.22 dB), 2.83 GHz (S_{11}=-18.76 dB) and 8.51 GHz (S_{11}=-33.42 dB) as shown in Fig. 5(b). In this case, the introduction of a fourth pin lowers the distance of the two lowest peaks to 400 MHz (the difference in frequency is related to the asymmetry of the pins along the X-axis direction that is necessary to achieve impedance matching). At the same time, these peaks are originated by the two halves of the external rectangular patch as demonstrated by the current density shown in Fig. 6. The two resonant modes irradiate providing a good radiation efficiency and impedance matching. The reflection coefficient is less than -10 dB for both frequencies.

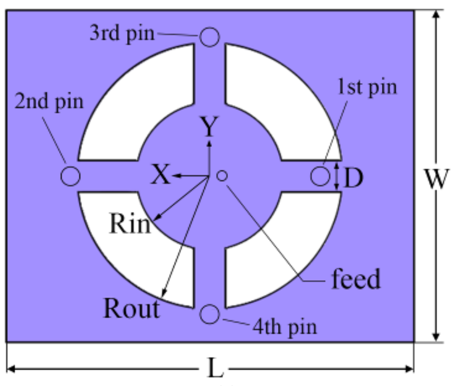

(a)

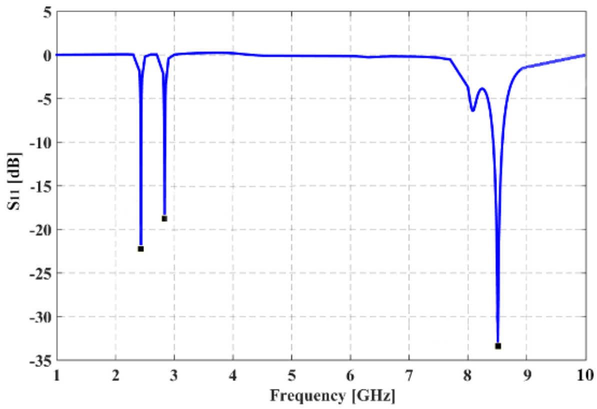

(b)

Figs. 5. Patch antenna with four shorting pins: (a) geometry; (b) computed scattering parameter S_{11}

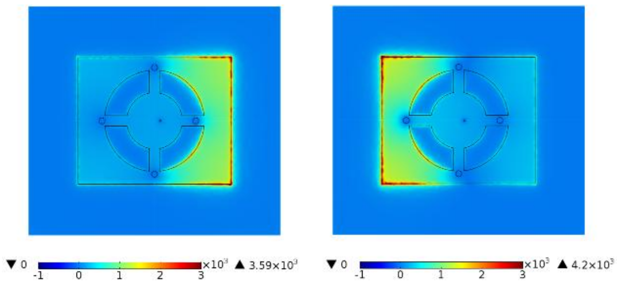

Fig. 6. Computed current density absolute magnitude (A/m^2) of the four-pin patch antenna at 2.43 GHz (left image) and 2.83 GHz (right image)

Figs. 7 depict the 2D patterns that show a total maximum antenna gain equal to 4.44 dBi, 6.31 dBi and 9.46 dBi computed at 2.43 GHz, 2.83 GHz, and 8.51 GHz, respectively. The E-plane computed at lower resonances, i.e. 2.43 GHz (Fig. 7(a)) and 2.83 GHz (Fig. 7(b)) is perfectly matched with the one expected by a patch antenna.

The H-plane shows an inclination of the main lobe caused by the asymmetry in the current density, i.e. the two halves shown in Fig. 6. Since these two halves of the rectangular patch create the resonances at lower frequencies, the main lobe direction at these frequencies is oblique with an angle of about 45 degrees for the 2.43 GHz and 15 degrees for the 2.83 GHz frequency with respect to the YZ-plane.

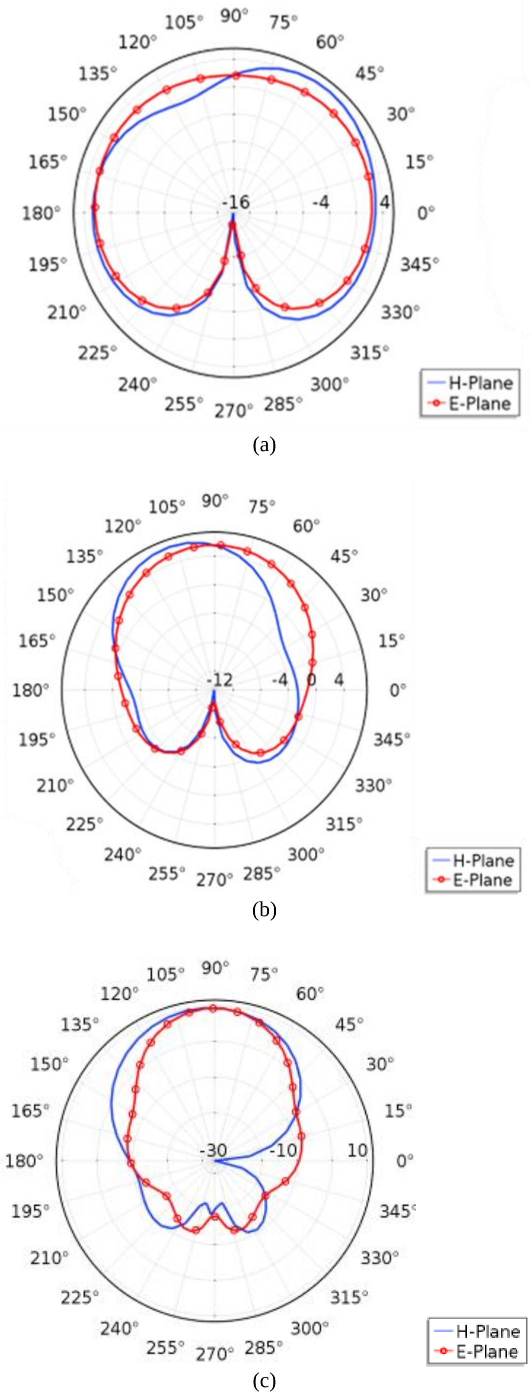

Figs. 7. 2D radiation pattern of the four-pin patch antenna computed at 2.43 GHz (a), 2.83 GHz (b) and 8.51 GHz (c). The beamwidth on the H-plane is about 170 degrees at 2.43 GHz, 75 degrees at 2.83 GHz and 55 degrees at 8.51 GHz

The inclination is symmetrical respect to the Y-axis, thus the maximum gain mainly points along the direction opposite to the plane YZ that defines also the symmetry of the antenna. The difference in the value of the antenna gain and the resonance frequency is likely because the first pin is still inside the bridge, a necessary condition to avoid the arising of the unwanted spurs on the reflection coefficient. In order to complete the analysis, the maximum realized antenna gain as function of frequency has been also computed and depicted in Figs. 8. In conclusion, the three-pin and the four-pin antennas show similar performance, as summarized in Table I.

Moreover, both antennas exhibit multi-band capability with three different resonances. However, the three-pin antenna is more attractive because the main lobe direction depends on the third pin position and the corresponding bridge respect to the X-axis as shown in Figs. 2. No similar behavior has been observed for the four-pin antenna.

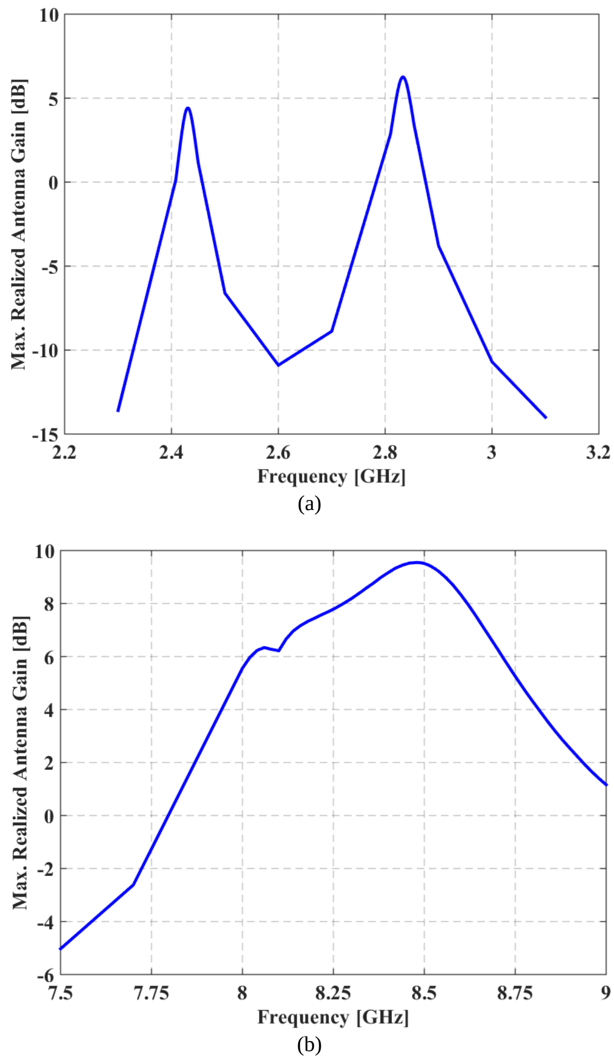

Figs. 8. Maximum realized antenna gain as function of lower frequencies (a) and higher frequencies (b) computed for the four-pin patch antenna

TABLE I
PERFORMANCE COMPARISON OF THE ANTENNAS

Parameter	Unit	Three-pin	Four-pin
First resonance (f_1)	GHz	2.187	2.431
Second resonance (f_2)	GHz	3.492	2.834
Third resonance (f_3)	GHz	9.4	8.51
S_{11} at f_1	dB	-12.75	-22.22
S_{11} at f_2	dB	-17.55	-18.76
S_{11} at f_3	dB	-35.72	-33.42
Max. antenna gain at f_1	dBi	3.84	4.44
Max. antenna gain at f_2	dBi	6.6	6.31
Max. antenna gain at f_3	dBi	9.83	9.46

III. Beam-Steering Capability Based on Graphene

In this section, it is discussed how to achieve beam-steering exploiting graphene-based shorting elements in the three-pin antenna configuration. Recent studies have shown that combining the use of thionyl chloride ($SOCl_2$) chemical doping and multilayer graphene, it is possible to control the sheet resistance so that the graphene is in a quasi-metallic region and acts as an optically transparent metal [28].

Combining such a property with the voltage-dependency of the graphene conductivity [30], an innovative reconfigurable antenna based on the three-pin patch antennas depicted in Figs. 2 has been designed. In this configuration, the copper bridges and their electrical connections to the ground plane have been substituted with graphene foils.

The graphene capability to operate in both quasi-metallic and lossy-dielectric region [28] has been exploited to control the direction of the maximum antenna gain.

The beam steering is obtained by controlling the graphene sheet resistance that can be reduced by applying a sufficient voltage across the graphene foils. If the sheet resistance is reduced such that it is smaller than the critical value ($\eta_0/2$ with η_0 corresponding to the impedance of free space), the graphene enters in the quasi-metallic region and behaves like a conductor replicating the behavior of the copper. In this paper, a graphene sheet resistance range from 20 (quasi-metallic) to 6000 Ω/sq (lossy dielectric) has been considered. The proposed solution is depicted in Figs. 9.

Four graphene foils are foreseen: two for the tuning of the bridges on the top patch (Fig. 9(a)) and two for the pin islands on the bottom ground plane (Fig. 9(b)) to control its electrical connection with the top bridges. Such antenna configuration allows three possible states:

- Irradiation of the three-pin antenna (case of Fig. 2(a), Y>0) by applying a voltage on the graphene bridge and island in the Y>0 section of the antenna;
- Irradiation of the three-pin antenna (case of Fig. 2(b), Y<0) by applying a voltage on the graphene bridge and island in the Y<0 section of the antenna;
- Irradiation of the four-pin antenna by applying a voltage to both graphene bridges and islands in the Y>0/Y<0 sections of the antenna.

The proposed graphene-based antenna has been implemented in COMSOL modeling the graphene foils using the aforementioned experimental values of the sheet resistance.

Such values of the sheet resistance affect the antenna performance since it impacts on the electric field according to the Ohm Law (1):

$$\mathbf{J} = \sigma \mathbf{E} \tag{1}$$

where σ is the graphene conductivity ($\sigma=1/R_s$). The area of the top foils is 2.4×2.75 mm^2 (its width is equal to the bridge width) while the size of the ones on the ground plane is 3×3 mm^2. Fig. 10 depicts the simulation results showing the 3D radiation pattern at 3.5 GHz. When a voltage is applied, i.e. when the sheet resistance is changed for example from 30 to 6000 Ω/sq, the antenna behaves like the two three-pin antennas shown in Fig. 2, proving the beam-steering capability as a function of the sheet resistance.

A correlation between the maximum antenna gain and the sheet resistance can be seen. Respect to the case shown in Figs. 2 (where the metal has been modeled as PEC), the gain is decreased to about 0 dBi. This reduction can be justified by considering the finite value of the graphene conductivity.

The antenna gain can be increased up to 1.41 dBi when the sheet resistance is 20 Ω/sq. Finally, Fig. 11 compares the S-parameters evaluated when the sheet resistance of the graphene equal to 20 and 30 Ω/sq is assumed.

The plot shows that the scattering parameter S_{11} is not affected by the change of the sheet resistance of the graphene at 3.5 GHz while the two curves differ at higher frequencies (e.g. 4.1 GHz).

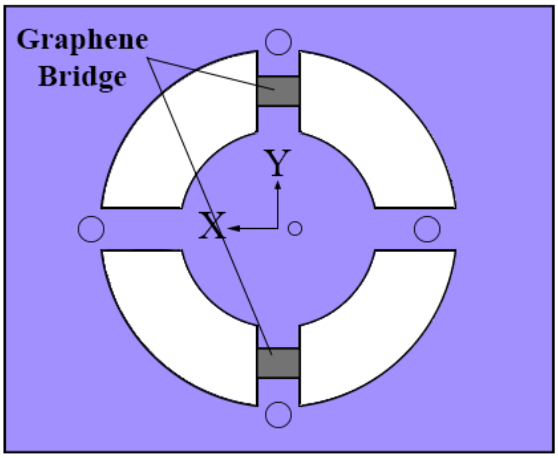

(a)

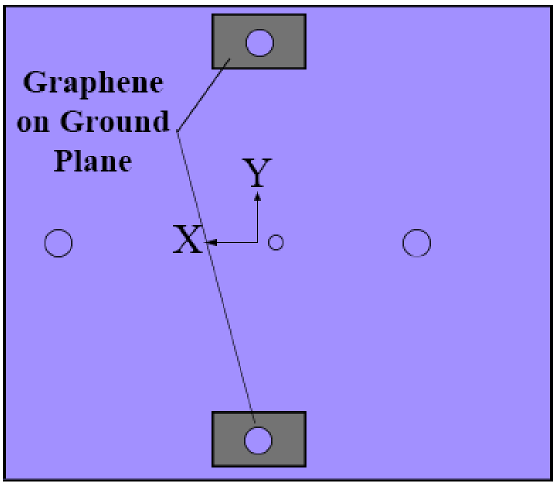

(b)

Figs. 9. Proposed solution for the graphene-based antenna: (a) top view; (b) bottom view

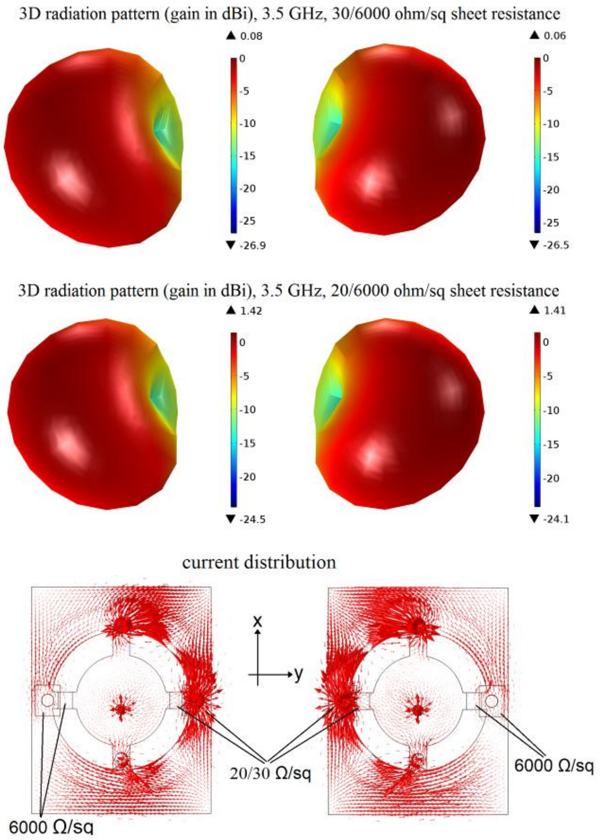

Fig. 10. 3D radiation patterns (top view) computed at 3.5 GHz. Left patterns are generated when voltages are applied on graphene foils in Y>0 sections; right ones when voltages are applied on graphene foils in Y<0 sections. The voltage application has been simulated by modifying the graphene sheet resistance from 30 to 6000 Ω/sq (two top images) and from 20 to 6000 Ω/sq (two center images). Two bottom images show the current distribution (top view) after the application of the voltage

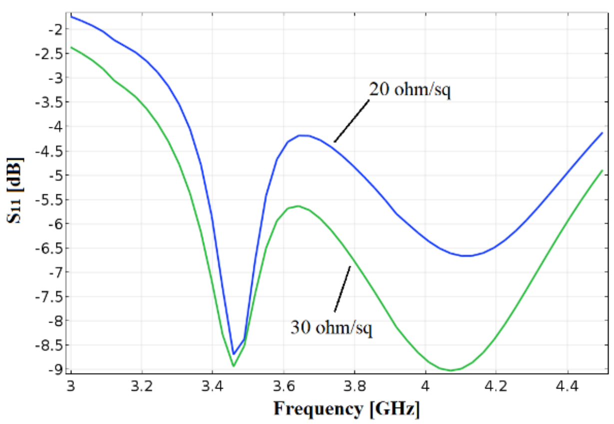

Fig. 11. Graphene-based antenna S_{11} parameter computed for 20 (blue curve) and 30 Ω/sq (green curve) sheet resistance

IV. Conclusion

In this paper, the design of a graphene-controlled reconfigurable antenna, which exploits three and four shorting pins, has been reported. It has been shown that the shorting pins give the antenna new features such as multi-band and beam-steering. Both antennas exhibit a multi-band behavior. However, the three-pin antenna has also the beam-steering capability that depends on the shorting elements, especially the third pin location. A steering of about 22 degrees in terms of radiation pattern orientation has been demonstrated. The electronic control of the beam has been obtained using graphene foils for the shorting elements. A solution that implements the presence/absence of the third shorting pin by controlling its electrical connection to the ground plane has been discussed. Two 2.4×2.75 mm^2 graphene foils have been used for the top bridges and two 3×3 mm^2 graphene foils have been used on the ground plane. Through numerical simulations, the beam-steering operation obtaining 1.41 maximum antenna gain when the graphene sheet resistance is fixed equal to 20 Ω/sq has been shown. The antenna gain could be further increased by gaining more knowledge about the graphene. As demonstrated, the antenna gain depends on the graphene size and the sheet resistance, therefore the possibility to improve the graphene doping and growth will in turn improve the antenna performance. At the same time, the proposed approach could be applied in different configurations in order to increase the number of beam directions or to control the beam width. The presented antenna could be suitable for the 5G applications thanks to its reconfigurable behavior introduced by the presence of graphene sheets. The exceptional property of this material and the innovative proposed antenna configuration could help to overcome the limitations related to the propagation losses, interferences, and so on, that will be the new challenges of the future 5G networks.

Acknowledgements

The Ph.D. student A. Lovascio benefits from a PhD MIUR fellowships for the 2018/2019 academic year, course XXXII, awarded within the framework of the “Programma Operativo Nazionale Ricerca e Innovazione” (PON RI 2014/2020) Axis I “Investments in Human Capital” - Action I.1– “Innovative PhDs with industrial characterization.” Funding FSE-FESR.

References

[1] Osseiran, Afif, J. F. Monserrat, P. Marsch, eds. *5G mobile and wireless communications technology*. Cambridge University Press, 2016.

[2] Cisco, *Visual Networking Index*, Feb. 2014, White Paper at Cisco.com.

[3] K. Tekkouk, J. Hirokawa, M. Ando, R. Sauleau, Continuous Beam Steering Antenna with Large 2D Coverage for 5G Applications, *2017 IEEE International Symposium on Antennas and Propagation & USNC/URSI National Radio Science Meeting.* IEEE, 2017.
doi: https://doi.org/10.1109/APUSNCURSINRSM.2017.8072164

[4] Kumar, P., Single Feed Dual Polarized Patch Antennas for Ultra-Wideband Applications, (2019) *International Review of Electrical Engineering (IREE)*, 14 (4), pp. 284-290.
doi: https://doi.org/10.15866/iree.v14i4.16154

[5] El Ayachi, M., Brachat, P., Rahmoun, M., New Electromagnetic

Band Gap Structure for Planar Low Profile Antenna with Wide Bandwidth and High Gain, (2018) *International Journal on Communications Antenna and Propagation (IRECAP)*, 8 (5), pp. 385-389.
doi: https://doi.org/10.15866/irecap.v8i5.14033

[6] Bandi, S., Sudhakar, A., Padma Raju, K., A Microstrip Rectangle Carpet Shaped Fractal Antenna for UWB Applications, (2016) *International Journal on Communications Antenna and Propagation (IRECAP)*, 6 (2), pp. 111-115.
doi: https://doi.org/10.15866/irecap.v6i2.8541

[7] Mahmoud, N., Hamad, E., Compact Dual Band-Notched Characteristics UWB Antenna Using Nested G-Shaped Slots, (2016) *International Journal on Communications Antenna and Propagation (IRECAP)*, 6 (5), pp. 282-290.
doi: https://doi.org/10.15866/irecap.v6i5.10001

[8] Nataraj, D., Karunakar, G., Compact Printed Elliptical Microstrip Patch with Defected Ground Structure (DGS) for Wireless Applications, (2018) *International Journal on Communications Antenna and Propagation (IRECAP)*, 8 (3), pp. 271-276.
doi: https://doi.org/10.15866/irecap.v8i3.12858

[9] Vasanthi, M., Srigayathri, V., Design and Simulation of Tri-Band Active Automotive Antenna, (2016) *International Journal on Communications Antenna and Propagation (IRECAP)*, 6 (4), pp. 226-231.
doi: https://doi.org/10.15866/irecap.v6i4.9408

[10] Singh, V., Mishra, B., Pandey, A., Patel, A., Yadav, S., Singh, R., Triple Band CPW Fed Monopole Leaf Shaped Patch Antenna, (2017) *International Journal on Communications Antenna and Propagation (IRECAP)*, 7 (2), pp. 135-141.
doi: https://doi.org/10.15866/irecap.v7i2.11842

[11] Alja'afreh, S., Folded Strip Monopole with SRR for Triple-Band Mobile Phone Applications, (2017) *International Journal on Communications Antenna and Propagation (IRECAP)*, 7 (7), pp. 613-618.
doi: https://doi.org/10.15866/irecap.v7i7.13208

[12] M. A. Hassanien, M. Jenning, D. Plettemeir, Beam Steering System using Rotman lens for 5G Applications at 28 GHz, *2017 IEEE International Symposium on Antennas and Propagation & USNC/URSI National Radio Science Meeting.* IEEE, 2017.
doi: https://doi.org/10.1109/APUSNCURSINRSM.2017.8073088

[13] K. Klionovoski, A. Shamim, M. S. Sharawi, 5G Antenna Array with Wide-Angle Beam Steering and Dual Linear Polarizations, *2017 IEEE International Symposium on Antennas and Propagation & USNC/URSI National Radio Science Meeting.* IEEE, 2017.
doi: https://doi.org/10.1109/APUSNCURSINRSM.2017.8072777

[14] M. K. Khattak, S. Kahng, M. S. Khattak, A. Rehman, C. Lee, D. Han, A Low profile, Wideband and High Gain Beam-steering Antenna for 5G Mobile Communication, *2017 IEEE International Symposium on Antennas and Propagation & USNC/URSI National Radio Science Meeting.* IEEE, 2017.
doi: https://doi.org/10.1109/APUSNCURSINRSM.2017.8073330

[15] J. Liu, Z. Tang, Z. Wang, H. Liu, Y. Yin, Gain Enhancement of a Broadband Symmetrical Dual-Loop Antenna Using Shorting pins, *IEEE Antennas and Wireless Propagation Letters 17.8* (2018): 1369-1372.
doi: https://doi.org/10.1109/LAWP.2018.2844293

[16] A. C. O. Pedra, G. Bulla, P. Serafini, A. A. A. de Salles, Shorting Pins Application in Wide-Band E-Shaped Patch Antenna, *2009 SBMO/IEEE MTT-S International Microwave and Optoelectronics Conference (IMOC)*. IEEE, 2009.
doi: https://doi.org/10.1109/IMOC.2009.5427591

[17] G. Zhou. (1998). Shorting-Pin Loaded Annular Ring Microstrip Antenna. *IEEE Antennas and Propagation Society International Symposium. 1998 Digest. Antennas: Gateways to the Global Network. Held in conjunction with: USNC/URSI National Radio Science Meeting* (Cat. No. 98CH36). Vol. 2. IEEE, 1998.
doi: https://doi.org/10.1109/APS.1998.702094

[18] S. H. S. Esfahlani, A. Tavakoli, P. Dehkhoda, A Compact Single-Layer Dual-Band Microstrip Antenna for Satellite Applications, *IEEE antennas and wireless propagation letters* 10 (2011): 931-934.
doi. https://doi.org/10.1109/LAWP.2011.2167121

[19] A. K. Singh, M. K. Meshram, Shorted Rectangular Microstrip Antenna for Dual-band Operation, *2006 IEEE Antennas and Propagation Society International Symposium.* IEEE, 2006.
doi: https://doi.org/10.1109/APS.2006.1711149

[20] X. Liu, Y. Li, Y. Wang, A Multi-band Square Patch Antenna Based on Shorted Pins and Asymmetric-circular Shaped Slots, *2016 Progress in Electromagnetic Research Symposium (PIERS)*. IEEE, 2016.
doi: https://doi.org/10.1109/PIERS.2016.7734849

[21] Nair R R, Blake P, Grigorenko A N, Novoselov K S, Booth T J, Stauber T, Peres N M R and Geim A K. (2008). Fine structure constant defines visual transparency of graphene. *Science*, 320 1308.
doi: https://doi.org/10.1126/science.1156965

[22] Grande, M., Bianco, G. V., Capezzuto, P., Petruzzelli, V., Prudenzano, F., Scalora, M., D'Orazio, A. (2018). Amplitude and phase modulation in microwave ring resonators by doped CVD graphene. *Nanotechnology*, 29(32).
doi: https://doi.org/10.1088/1361-6528/aac557

[23] C. Shi, I. J. Luxmoore, G. R. Nash. (2009). Gate tunable graphene-integrated metasurface modulator for mid-infrared beam steering. *Optics Express*, vol.27, n.10, 13 May 2019,14577-14584.
doi: https://doi.org/10.1364/OE.27.014577

[24] Zhang Zhang, Xin Yan, Lanju Liang, Dequan Wei, Meng Wang, Yaru Wang, Jianquan Yao: The novel hybrid metal-graphene metasurfaces for broadband focusing and beam-steering in farfield at the terahertz frequencies. *Carbon*, Volume 132, June 2018, Pages 529-538.
doi: https://doi.org/10.1016/j.carbon.2018.02.095

[25] B. Orazbayev, M. Beruete, and I. Khromova, Tunable beam steering enabled by graphene metamaterials, *Opt. Express* 24, 8848-8861 (2016).
doi: https://doi.org/10.1364/OE.24.008848

[26] Miao Z, Wu Q, Li X, He Q, Ding K, An Z, Zhang Y and Zhou L.: Widely tunable terahertz phase modulation with gate-controlled graphene metasurfaces, *Phys. Rev. X* 5 041027, 2015.
doi: https://doi.org/10.1103/PhysRevX.5.041027

[27] Sensale-Rodriguez B, Yan R, Kelly M M, Fang T, Tahy K, Hwang W S, Jena D, Liu L and Xing H G: Broadband graphene terahertz modulators enabled by intraband transitions *Nat. Commun.* 3 780, 2012.
doi: https://doi.org/10.1038/ncomms1787

[28] M. Grande, G. V. Bianco, M. A. Vincenti, D. de Ceglia, P. Capezzuto, M. Scalora, A. D'Orazio, G. Bruno, Optically Transparent Microwave Polarizer Based on Quasi-Metallic Graphene, *Scientific reports* 5 (2015): 17083.
doi: https://doi.org/10.1038/srep17083

[29] Wu B, Tuncer H M, Naeem M, Yang B, Cole M T, Milne W I and Hao Y: Experimental demonstration of a transparent graphene millimetre wave absorber with 28% fractional bandwidth at 140GHz, *Sci. Rep.* 4 4130, 2014.
doi: https://doi.org/10.1038/srep04130

[30] Grande, M., Bianco, G.V., Perna, F.M.,Capriati V., Capezzuto P., Scalora M., Bruno, G., D'Orazio, A.: Reconfigurable and optically transparent microwave absorbers based on deep eutectic solvent-gated graphene, *Scientific Reports*, 9, art. number 5463, 2019.
doi: https://doi.org/10.1038/s41598-019-41806-w

[31] Grande M, D'Orazio A, Bianco G V, Bruno G, Vincenti M A, de Ceglia D and Scalora M 2015 Optically transparent graphene-based Salisbury screen microwave absorber *IEEE 15th Mediterranean Microwave Symp. (MMS)*.
doi: https://doi.org/10.1109/MMS.2015.7375386

[32] Balci O, Polat E O, Kakenov N and Kocabas C: Graphene-enabled electrically switchable radar-absorbing surfaces, *Nat. Commun.* 6 6628, 2015.
doi: https://doi.org/10.1038/ncomms10000

[33] Grande M, Bianco G V, Vincenti M A, de Ceglia D, Capezzuto P, Petruzzelli V, Scalora M, Bruno G and D'Orazio A: Optically transparent microwave screens based on engineered graphene layers *Opt. Express* 24 22788–95, 2016.
doi: https://doi.org/10.1364/OE.24.022788

[34] Grande, M., Bianco, G. V., Laneve, D., Capezzuto, P., Petruzzelli, V., Scalora, M., D'Orazio, A. (2018). Optically

transparent wideband CVD graphene-based microwave antennas. *Applied Physics Letters*, 112(25).
doi: https://doi.org/10.1063/1.5037409

[35] Perruisseau-Carrier J.: Graphene for antenna applications: Opportunities and challenges from microwaves to THz, *2012 Loughborough Antennas and Propagation Conf. (LAPC)* (Loughborough) pp 1–4, 2012.
doi: https://doi.org/10.1109/LAPC.2012.6402934

[36] Hend. A. Malhat, Saber H. Zainud-Deen, Shaymaa M.Gaber: Graphene based transmitarray for terahertz applications, *Progress in electromagnetics research M*, vol.36, 185-191, 2014.
doi: https://doi.org/10.2528/PIERM14050705

[37] A. Lovascio, M. Grande, A. D'Orazio (2019). Design of a Dual-Frequency Patch Antenna for Small Satellites. In *8th European Conference for Aeronautics and Space Sciences (EUCASS)*.

Authors' information

[1]Dipartimento di Ingegneria Elettrica e dell'Informazione, Politecnico di Bari, 4, E. Orabona, St., Bari, Italy.

[2]Space Instrument & Avionic Division, Sitael S.p.A., 21, San Sabino St., Mola di Bari, Italy.

A. Lovascio was born in Bitonto, Italy, on 28th April, 1989. From Politecnico di Bari, Italy, he received his bachelor's degree in Electronic Engineering and his master's degree with Honors in Telecom Engineering and the title of Research Doctor in Electrical and Information Engineering in 02-2020. During the PhD course he was engaged in research on RF systems and devices for the aerospace. Since January 2020 he has held the position of Satellite Electrical Architect at Sitael – Mola di Bari.
E-mail: antonio.lovascio@poliba.it

A. D'Orazio ('58) received the laurea degree in Electrical Engineering, summa cum laude, from the University of Bari in 1983 and the Ph.D. degree in Electromagnetisms in 1987. She has been Assistant Professor ('90), associate professor ('98), full professor of Electromagnetic Fields of Politecnico di Bari (2003). Member of the Management Committee of the European COST actions 268 and 288. Depute Chancellor of Politecnico di Bari and member of the Board of Governors (2003). Member of the Executive Board of the "ARTI - Regione Puglia. Coordinator of the PhD Course in Electronic Engineering (2004-2009). Since 2011 she is member of the Management Committee of CNIT. Since 2003 she acts as an Expert Reviewer of projects financed by MIUR, European Commission (VII FP and Horizon 2020), by Apulia region. Principal Investigator of research projects funded by MIUR and research contracts funded by National and International companies. She was involved in the COST Actions 268, 288, P11, MP0702, MP0805. Component of scientific committees of national and international conferences. Member of IEEE, OSA, AEIT, SIEm. The research concerning the design, fabrication and characterization of microwave and optical devices, antennas and graphene-based devices, is documented by more than 300 publications published on international journals and conference proceedings, invited papers.
E-mail: antonella.dorazio@poliba.it

M. Grande received the laurea degree in Electronic Engineering, summa cum laude, and the PhD degree from Politecnico di Bari in 2006 and 2010, respectively. From February 2006 to February 2008, he visited the National Nanotechnology Laboratory (NNL) while from February 2008 to April 2009 he has been a visiting student at School of Physics and Astronomy of the St Andrews University (Scotland) working on the design, the fabrication and the characterization of Photonic Crystals. Since October 2015 he is Assistant Professor at Politecnico di Bari in Electromagnetic Fields. His research interests include photonic crystals, plasmonic nanostructures and graphene-based devices operating in both optical and microwave regimes.
E-mail: marco.grande@poliba.it